Contribution from the Institut für Physik, Medizinische Universität, Ratzeburger Allee 160, D-2400 Lübeck, FRG, and Laboratoire de Cristallochimie et de Chimie Structurale, URA (CNRS) 424, Institut le Bel, Université Louis Pasteur, 4 Rue B. Pascal, F-67070 Strasbourg, France

Six-Coordinate Quantum-Mechanically Weakly Spin-Mixed ($S = {}^5/_2, {}^3/_2$) (Triflato)aquoiron(III) "Picket-Fence" Porphyrin Complex: Synthesis and Structural, Mössbauer, EPR, and Magnetic Characterization

A. Gismelseed,[1] E. L. Bominaar,[1] E. Bill,[1] A. X. Trautwein,*[,1] H. Winkler,[1] H. Nasri,[2] P. Doppelt,[2] D. Mandon,[2] J. Fischer,[2] and R. Weiss*[,2]

Received November 2, 1988

The iron(III) "picket-fence" porphyrin complex [$Fe^{III}(TP_{piv}P)(OSO_2CF_3)(H_2O)$] (**1**) was synthesized and characterized by its UV–visible, ^1H NMR, EPR, magnetic, and Mössbauer properties. The X-ray structure of **1** was determined at −100 °C. Crystal data: [$Fe(TP_{piv}P)(OSO_2CF_3)(H_2O)$] ($C_{65}H_{66}N_8O_8F_3SFe$); monoclinic; a = 13.161 (3), b = 19.196 (6), c = 26.212 (6) Å; β = 103.34 (2)°; Z = 4; d_{calc} = 1.270 g cm^{-3}; space group $P2_1/c$. The six-coordinate iron atom is bonded to the four porphyrinato nitrogens (Fe–N_p = 2.021 (16) Å), to an oxygen atom of the triflate ion (Fe–O(triflate) = 2.188 (5) Å), placed inside the molecular cavity of the picket-fence porphyrin, and to a water molecule (Fe–O(water) = 2.133 (5) Å). The susceptibility measurements in an external field of 1.5 T show that the effective magnetic moment varies from 4.0 to 5.7 μ_B in the temperature range 2–300 K. The EPR data yield $g_\perp$ = 5.7, which corresponds to a mixture of 85% spin sextet $^6A_1$ and 15% spin quartet $^4A_2$ in the lowest Kramers doublet. This mixture is somewhat stronger than in typical high-spin iron porphyrins. Mössbauer spectra were recorded at temperatures varying from 4.2 to 300 K in fields of 0–6.21 T. They exhibit temperature-independent quadrupole splitting, $\Delta E_Q \approx 2.2$ mm s^{-1}, which lies between the ΔE_Q values characteristic for high-spin ($S = {}^5/_2$) and intermediate-spin ($S = {}^3/_2$) porphyrins. The magnetic hyperfine patterns of the measured Mössbauer spectra, in the slow and fast relaxation limit, are successfully simulated within the 10-state model for the spin mixture between $^6A_1$ and $^4A_2$ by using parameters that have been derived from susceptibility and EPR data within the same model. The applicability of the usual spin ($S = {}^5/_2$) Hamiltonian analysis and its relation to the 10-state model are discussed. Spin–spin and spin–lattice relaxation effects are explicitly accounted for in the intermediate relaxation regime within the framework of the ($S = {}^5/_2$) spin Hamiltonian. The degree of spin mixture together with the axial and porphyrinato-nitrogen coordination of iron in **1** and related complexes is discussed on the basis of a putative spin-state/stereochemical relationship.

Introduction

Several intermediate-spin ($S = {}^3/_2$) and quantum-mechanically mixed-spin ($S = {}^5/_2, {}^3/_2$) porphyrin derivatives have been studied during the last 10 years.[3-9] Among these compounds, three six-coordinate species with two identical axial ligands, [Fe(TPP)(C(CN)$_3$)$_2$]$_n$, [Fe(OEP)(3-Cl-py)$_2$]$^+$ (monoclinic form), and [Fe(OEP)(THF)$_2$], have been completely characterized.[4-6] We have now synthesized the iron(III) triflate "picket-fence" porphyrin complex containing a water molecule as second axial ligand and find that the $S = {}^5/_2$ spin state is weakly quantum-mechanically mixed with the $S = {}^3/_2$ spin state. We report here the preparation, structure, and spectroscopic and magnetic properties of this (triflato)aquoiron(III) picket-fence porphyrin derivative.

Experimental Section

All preparations were carried out in Schlenk tubes under argon. Pentane was dried by distillation over CaH_2. THF and *n*-hexane were dried and degassed under argon by distillation over sodium/benzophenone. [$Fe(TP_{piv}P)(Cl)$] was prepared by literature methods.[10] Silver triflate was purchased from Jansen Chemicals and used as such. It contained small quantities of water, which were not removed.

Synthesis of [$Fe(TP_{piv}P)(OSO_2SF_3)(H_2O)$] (1). To a THF solution (150 mL) of [$Fe(TP_{piv}P)Cl$] (100 mg, 91 mmol) was added a THF solution (10 mL) of silver triflate (23.5 mg, 91 mmol). The resulting brown-red solution was stirred under argon for 12 h at room temperature and then filtered. Hexane (30 mL) was then added under continuous swirling. The solution was then slowly concentrated under vacuum until precipitation of **1** occurred in the form of small crystals. λ_{max} (log ϵ) (C_6H_5Cl): 412 (5.20), 513 (4.92), 572 (3.79), 645 nm (3.24). ^1H NMR ($CHCl_3$): δ_{pyr} = 30.4 ppm/TMS.

The unit-cell parameters determined with a small crystal of **1**, obtained as indicated above, are identical with those of the crystals prepared by slow diffusion of pentane into chlorobenzene solutions of the compound.

X-ray Crystallography. A systematic search in reciprocal space with a Philips PW1100/16 automatic diffractometer showed that crystals of **1** belong to the monoclinic system. The unit-cell dimensions and their standard deviations were obtained and refined at −100 °C (achieved by using a locally built gas-flow system) with Cu Kα radiation (λ = 1.5405 Å) by using 25 carefully selected reflections and the standard Philips software. Final results are as follows: $C_{65}H_{66}N_8O_8F_3SFe$; MW = 1232.2; a = 13.161 (3), b = 19.196 (6), c = 26.212 (6) Å; β = 103.34 (2)°; V = 6443.3 Å^3, Z = 4, d_{calc} = 1.270 g cm^{-3}, μ = 27.223 cm^{-1}, $F(000)$ = 2580, space group $P2_1/c$. A nearly parallelepipedic crystal of dimensions 0.45 × 0.20 × 0.15 mm^3 was cut out of a cluster of crystals, glued at the end of a glass wire, and mounted on a rotation-free goniometer head. All quantitative data were obtained from a Philips PW1100/16 automatic diffractometer, at −100 °C, controlled by a P852 computer, using graphite-monochromated radiation and standard software. The vertical and horizontal apertures in front of the scintillation counter were adjusted so as to minimize the background without loss of net peak intensity at the 2σ level. The total scan width ($\theta/2\theta$ flying step-scan mode) used was $\Delta w = (1.2 + 0.143 \tan\theta)°$ with a step width of 0.05° and a scan speed of 0.024° s^{-1}. A total of 9027 ($\pm h,k,l$) reflections were recorded (4° < θ < 57°). The resulting data set was transferred to a MicroVax II computer, and for all subsequent computations, the Enraf-Nonius SDP/VAX package[11] was used with the exception of a local data-reduction program. Three standard reflections measured every 1 h during the entire data-collection period showed no significant trend. The raw step-scan data were converted to intensities by using the Lehmann–Larsen method[12] and then corrected for Lorentz and polarization factors. Absorption corrections were computed by using

(1) Medizinische Universität.
(2) Université Louis Pasteur.
(3) Dolphin, D. H.; Sams, J. R.; Tsin, T. B. *Inorg. Chem.* **1977**, *16*, 711.
(4) Summerville, D. A.; Cohen, I. A.; Hatano, K.; Scheidt, W. R. *Inorg. Chem.* **1978**, *17*, 2906.
(5) Scheidt, W. R.; Geiger, D. K.; Hayes, R. J.; Lang, G. *J. Am. Chem. Soc.* **1983**, *105*, 2625.
(6) Masuda, H.; Taga, T.; Osaki, K.; Sugimoto, H.; Yoshida, Z.; Ogoshi, H. *Bull. Chem. Soc. Jpn.* **1982**, *55*, 3891.
(7) Reed, C. A.; Mashiko, T.; Bentley, S. R.; Kastner, M. E.; Scheidt, W. R.; Spartalian, K.; Lang, G. *J. Am. Chem. Soc.* **1979**, *101*, 2948.
(8) Toney, G. E.; ter Haar, L. W.; Savrin, J. E.; Gold, A.; Hatfield, W. E.; Sangaiah, R. *Inorg. Chem.* **1984**, *23*, 2563.
(9) Toney, G. E.; Gold, A.; Savrin, J. E.; ter Haar, L. W.; Sangaiah, R.; Hatfield, W. E. *Inorg. Chem.* **1984**, *23*, 4350.
(10) Collman, J. P.; Gagné, R. R.; Halbert, T. R.; Lang, G.; Robinson, W. T. *J. Am. Chem. Soc.* **1975**, *97*, 1427.
(11) Frenz, B. A. In *Computing in Crystallography*; Schenk, H., Olthof-Hazekamp, R., van Koningsveld, H., Bassi, C. G., Eds.; Delft University Press: Delft, The Netherlands, 1978; p 65.
(12) Lehmann, M. S.; Larsen, F. K. *Acta Crystallogr., Sect. A: Cryst. Phys., Diffr., Theor. Gen. Crystallogr.* **1974**, *A30*, 580.

0020-1669/90/1329-2741$02.50/0

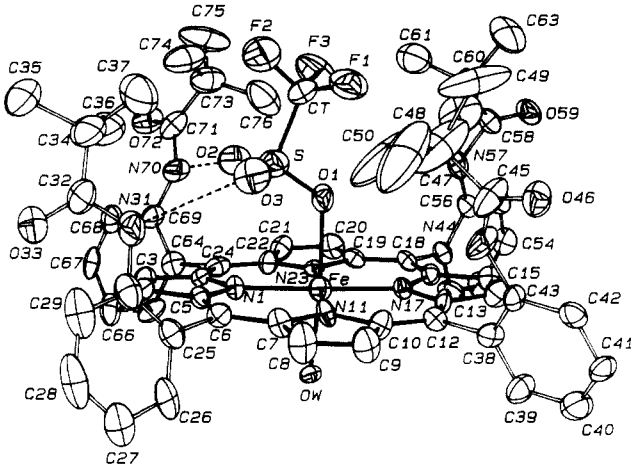

Figure 1. ORTEP plot, giving the numbering scheme used for [Fe($TP_{piv}P$)(OSO_2CF_3)(H_2O)] (**1**) and showing the surroundings of the iron atom, the position of the triflate ion inside the molecular cavity, and the two O···HN (triflate–pivalamido NH) hydrogen bonds. Thermal ellipsoids are at the 30% probability level.

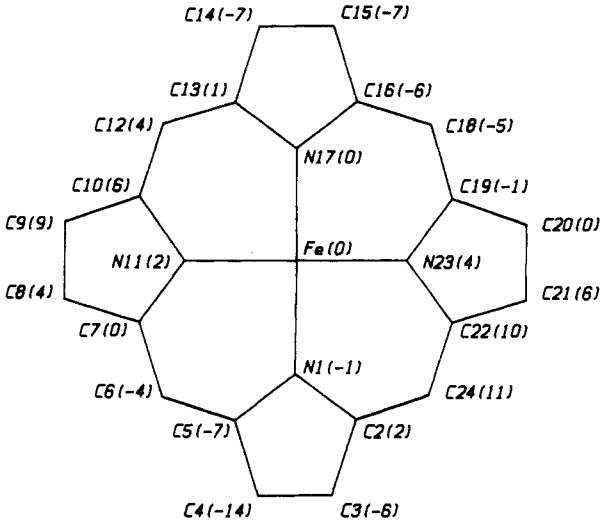

Figure 2. Formal diagram of the porphyrinato core. The numbers in parentheses indicate the perpendicular displacement for each atom in units of 0.01 Å from the mean plane of the 24-atom core.

the empirical method of Walker and Stuart[13] (transmission factors between 0.77 and 1.23). A unique data set of 4752 reflections having $I > 3\sigma(I)$ was used for determining and refining the structure. The poor ratio of observed/collected data indicates the occurrence of high thermal motion even at −100 °C and/or some minor disorder of the *tert*-butyl groups belonging to the four pivalamide pickets of the porphyrin. The structure was solved by Patterson and Fourier techniques. After refinement of the heavy atoms, a difference-Fourier map revealed maxima of electronic density close to the positions expected for hydrogen atoms; they were introduced in structure factor calculations by their computed coordinates (C–H = N–H = 0.95 Å) and isotropic temperature factors such that $B(H) = 1.3B_{eqv}$ (C or N) Å^2 but not refined (water hydrogens were omitted). Full least-squares refinement minimizing $\sum w(|F_o| - |F_c|)^2$ converged to $R(F) = 0.079$ and $R_w(F) = 0.104$ ($\sigma^2(F^2) = \sigma^2$(counts) + $(pI)^2$). The unit-weight observation was 1.358 for $p = 0.08$. A final difference map showed no significant maxima. The scattering factor coefficients and anomalous dispersion coefficients, respectively, come from parts a and b of ref 14.

Spectroscopic Methods. UV–visible spectra were obtained with a Cary 210 spectrometer. ^{1}H NMR spectra were measured on a Bruker SY200 instrument.

The EPR spectrometer was a conventional X-band apparatus (Bruker ER200D); the data acquisition system, based on a personal computer, is a local development. The spectrometer was equipped with a helium-flow cryostat (Oxford Instruments ESR10), which provided temperatures down to 2.5 K.

Magnetic susceptibilities were measured on a powder sample between 2 and 300 K by using a Foner susceptometer.

The Mössbauer spectrometer worked in conventional constant-acceleration mode with a source of 1.85 GBq ^{57}Co/Rh (Amersham Buchler). From calibration measurements we got a standard line width of 0.23 mm s^{-1}. Isomer shifts are given relative to metallic iron (α-Fe) at room temperature. The Mössbauer cryostats were a helium-bath cryostat (MD306, Oxford Instruments) and a superconducting magnet system with split coil geometry (Oxford Instruments). The γ-beam could be transmitted parallel or perpendicular to the field.

Molecular Structure of 1

Figure 1 displays a perspective view of the molecular structure of **1**. This figure also gives the labeling scheme used for all the atoms of this unit. Figure 2 shows a formal diagram of the porphyrinato core indicating the perpendicular displacements in units of 0.01 Å of each core atom from the mean plane of the 24-atom core. Atomic positional parameters are indicated in Table I, and selected interatomic distances and angles are presented in Table II. The six-coordinate iron atom is bonded to the four porphyrinato nitrogens, to an oxygen atom of the triflate anion, and to a water molecule. The triflate anion is located inside the molecular cavity of the "picket-fence" porphyrin. This type of structure, which is generally found when an anionic axial ligand is present, is probably related to the polarizing properties of the four pivalamide pickets.[15-17] The Fe–N_p distances range from 2.005 (2) to 2.039 (5) Å, and their mean value is 2.021 (16) Å. The iron–oxygen(triflate) bond distance of 2.188 (5) Å is clearly longer than the Fe–O bond length observed in the five-coordinate mixed-spin ($S = {}^5/_2, {}^3/_2$) perchlorato complexes [Fe(TPP)(ClO_4)] (2.029 (4) Å)[7] and [Fe(OEP)(ClO_4)] (2.067 (9) Å).[18] NMR studies of the mixed-spin five-coordinate complexes [Fe(TPP)(OSO_2CF_3)] and [Fe(TPP)(ClO_4)] indicate that the triflate ion is a stronger ligand than the perchlorate ion.[19] The increased Fe–O(triflate) bond length observed in **1** with respect to the Fe–O bond length formed in [Fe(TPP)(ClO_4)][7] may be related to six-coordination and/or to the weak hydrogen bonding between the triflate ion and the adjacent N–H groups of the pivalamide pickets (vide infra). The Fe–O(water) bond length of 2.133 (5) Å is also somewhat longer than the Fe–O(water) bond length observed in the six-coordinate high-spin iron(III) complex [Fe(TPP)(H_2O)$_2$]$^+$ (2.095 (2) Å).[20] Thus, the iron atom in **1** experiences a slightly increased tetragonal distortion relative to the high-spin species [Fe(TPP)(H_2O)$_2$]$^+$. The two Fe–O bonds in **1** are slightly tipped by 1.2 (3)° (triflate) and 4.4 (3)° (water), respectively, relative to the normal to the 24-core-atom mean plane. As indicated above, the triflate ion is located inside the molecular cavity of the picket-fence porphyrin and is hydrogen bonded to the two N–H groups of the adjacent pivalamide pickets (Figure 1). The corresponding distances of 3.241 (12) Å (O2···N31) and 3.368 (10) Å (O2···N70) indicate two weak hydrogen-bond interactions.[21] As is shown in Figure 2, the porphyrin core in **1** has a ruffled conformation. Agreement between chemically equivalent bond distances and bond angles within the porphyrin ring and the four pivalamide "pickets" are satisfactory. The mean values of the chemically equivalent bond distances and bond angles found in these units are given in Table II. The thermal parameters of the *tert*-butyl group attached to C45 (Figure 1) suggest the possibility

(13) Walker, N.; Stuart, D. *Acta Crystallogr., Sect A: Found. Crystallogr.* **1983**, *A39*, 158.
(14) (a) Cromer, D. T.; Waber, J. T. In *International Tables for X-Ray Crystallography*; Kynoch: Birmingham, England, 1974; Vol. IV, Table 2.2b. (b) *Ibid.*, Table 2.3.1.
(15) Schappacher, M.; Ricard, L.; Weiss, R.; Montiel-Montoya, R.; Gonser, U.; Bill, E.; Trautwein, A. X. *Inorg. Chim. Acta* **1983**, *78*, L9.
(16) Nasri, H.; Fischer, J.; Weiss, R.; Bill, E.; Trautwein, A. X. *J. Am. Chem. Soc.* **1987**, *109*, 2549.
(17) Bounab, B.; Ricard, L.; Fischer, J.; Weiss, R. Unpublished results.
(18) Masuda, H.; Taga, T.; Osaki, K.; Sugimoto, H.; Yoshida, Z. I.; Ogoshi, H. *Inorg. Chem.* **1980**, *19*, 950.
(19) Boersma, A. D.; Goff, H. M. *Inorg. Chem.* **1982**, *21*, 581.
(20) Scheidt, W. R.; Cohen, I. A.; Kastner, M. E. *Biochemistry* **1979**, *18*, 3546.
(21) Pimentel, G. C.; McClellan, A. L. In *The Hydrogen Bond*; W. H. Freeman: San Francisco, CA, 1960.

Table I. Positional Parameters and Their Estimated Standard Deviations

atom	x	y	z	B,[a] Å²	atom	x	y	z	B,[a] Å²
Fe	0.7752 (1)	0.22433 (7)	0.79455 (5)	2.58 (3)	C43	0.4734 (6)	0.0252 (5)	0.6782 (4)	2.2 (2)
N1	0.7673 (5)	0.2866 (4)	0.8561 (3)	2.1 (2)	N44	0.4973 (6)	0.0028 (5)	0.7299 (3)	3.7 (2)
C2	0.8495 (7)	0.3232 (5)	0.8860 (3)	2.2 (2)	C45	0.4564 (8)	−0.0497 (6)	0.7539 (4)	4.5 (3)
C3	0.8128 (7)	0.3585 (5)	0.9258 (4)	2.4 (2)	O46	0.3912 (5)	−0.0892 (4)	0.7294 (3)	3.5 (2)
C4	0.7112 (8)	0.3442 (5)	0.9207 (4)	2.9 (2)	C47	0.493 (1)	−0.0538 (8)	0.8123 (5)	10.1 (4)
C5	0.6818 (6)	0.3005 (4)	0.8761 (3)	2.0 (2)	C48	0.386 (2)	−0.038 (1)	0.8328 (6)	12.3 (6)
C6	0.5808 (7)	0.2768 (5)	0.8549 (4)	2.4 (2)	C49	0.518 (1)	−0.128 (1)	0.8250 (7)	11.6 (6)
C7	0.5520 (7)	0.2330 (5)	0.8111 (4)	2.6 (2)	C50	0.559 (2)	0.005 (1)	0.8380 (6)	13.7 (6)
C8	0.4482 (7)	0.2094 (6)	0.7898 (4)	3.9 (3)	C51	1.0553 (6)	0.1443 (5)	0.7102 (4)	2.3 (2)
C9	0.4534 (7)	0.1682 (6)	0.7473 (4)	3.6 (3)	C52	1.0808 (8)	0.1859 (5)	0.6734 (4)	3.6 (2)
C10	0.5596 (7)	0.1649 (5)	0.7425 (4)	2.8 (2)	C53	1.1558 (8)	0.1659 (6)	0.6469 (4)	3.9 (3)
N11	0.6188 (5)	0.2066 (4)	0.7829 (3)	2.0 (2)	C54	1.2047 (7)	0.1026 (6)	0.6575 (4)	3.5 (2)
C12	0.5960 (6)	0.1267 (5)	0.7062 (3)	2.0 (2)	C55	1.1805 (7)	0.0590 (5)	0.6938 (4)	3.0 (2)
C13	0.6991 (7)	0.1254 (5)	0.7032 (3)	2.4 (2)	C56	1.1043 (7)	0.0788 (5)	0.7210 (4)	2.5 (2)
C14	0.7382 (7)	0.0826 (6)	0.6669 (4)	3.2 (2)	N57	1.0752 (6)	0.0379 (4)	0.7604 (3)	3.3 (2)
C15	0.8417 (8)	0.0940 (5)	0.6743 (4)	3.0 (2)	C58	1.0831 (7)	−0.0337 (5)	0.7656 (4)	3.1 (2)
C16	0.8699 (7)	0.1416 (5)	0.715 (3)	2.1 (2)	O59	1.1248 (5)	−0.0713 (3)	0.7390 (3)	3.9 (2)
N17	0.7819 (5)	0.1604 (4)	0.7349 (3)	1.8 (2)	C60	1.0334 (8)	−0.0609 (5)	0.8090 (4)	3.5 (2)
C18	0.9722 (7)	0.1666 (5)	0.7378 (4)	2.5 (2)	C61	1.100 (1)	−0.0328 (7)	0.8642 (5)	5.9 (3)
C19	0.9979 (6)	0.2136 (5)	0.7790 (4)	2.1 (2)	C62	0.920 (1)	−0.0385 (8)	0.7797 (5)	6.9 (4)
C20	1.1003 (7)	0.2409 (5)	0.8004 (4)	3.2 (2)	C63	1.046 (1)	−0.1398 (6)	0.8115 (5)	7.7 (4)
C21	1.0945 (7)	0.2856 (5)	0.8393 (4)	3.1 (2)	C64	1.0218 (7)	0.3773 (5)	0.9141 (4)	2.7 (2)
C22	0.9887 (7)	0.2879 (5)	0.8423 (3)	2.3 (2)	C65	1.0085 (7)	0.4473 (6)	0.9002 (4)	3.3 (2)
N23	0.9292 (5)	0.2429 (4)	0.8056 (3)	1.8 (2)	C66	1.0660 (8)	0.4988 (5)	0.9333 (4)	3.9 (3)
C24	0.9518 (7)	0.3251 (5)	0.8787 (4)	2.5 (2)	C67	1.1306 (8)	0.4766 (6)	0.9798 (4)	3.5 (2)
C25	0.4948 (7)	0.3045 (5)	0.8774 (4)	2.8 (2)	C68	1.1450 (8)	0.4101 (6)	0.9927 (4)	3.6 (3)
C26	0.4245 (7)	0.3508 (5)	0.8459 (4)	3.7 (2)	C69	1.0915 (7)	0.3578 (5)	0.9608 (4)	2.8 (2)
C27	0.3447 (7)	0.3827 (6)	0.8639 (5)	4.4 (3)	N70	1.1009 (6)	0.2869 (4)	0.9726 (3)	3.4 (2)
C28	0.3355 (7)	0.3668 (6)	0.9145 (5)	5.0 (3)	C71	1.1848 (8)	0.2558 (6)	1.0060 (4)	3.9 (3)
C29	0.4050 (8)	0.3200 (6)	0.9467 (5)	4.8 (3)	O72	1.2578 (6)	0.2888 (4)	1.0321 (3)	4.7 (2)
C30	0.4861 (8)	0.2910 (5)	0.9282 (4)	3.6 (2)	C73	1.1812 (9)	0.1754 (7)	1.0077 (5)	5.2 (3)
N31	0.5559 (7)	0.2462 (5)	0.9606 (3)	4.2 (2)	C74	1.093 (1)	0.1550 (7)	1.0356 (5)	6.2 (4)
C32	0.6036 (9)	0.2632 (6)	1.0108 (4)	5.1 (3)	C75	1.288 (1)	0.1517 (8)	1.0405 (7)	8.7 (5)
O33	0.5924 (7)	0.3227 (5)	1.0273 (3)	6.3 (2)	C76	1.158 (1)	0.1438 (7)	0.9529 (6)	6.8 (4)
C34	0.675 (1)	0.2127 (7)	1.0442 (5)	6.5 (3)	S	0.8107 (2)	0.1384 (2)	0.9035 (1)	3.99 (7)
C35	0.672 (1)	0.2258 (8)	1.1033 (5)	7.7 (4)	O1	0.8102 (5)	0.1357 (3)	0.8482 (2)	3.2 (2)
C36	0.790 (1)	0.2268 (8)	1.0404 (5)	7.7 (4)	O2	0.8924 (6)	0.1820 (4)	0.9331 (3)	4.7 (2)
C37	0.643 (1)	0.1346 (8)	1.0287 (5)	8.3 (4)	O3	0.7046 (5)	0.1442 (4)	0.9113 (3)	5.0 (2)
C38	0.5185 (6)	0.0857 (5)	0.6661 (4)	2.4 (2)	CT	0.8494 (8)	0.0519 (6)	0.9261 (4)	3.6 (3)
C39	0.4963 (8)	0.1105 (6)	0.6140 (4)	3.5 (3)	F1	0.7968 (6)	0.0018 (3)	0.8987 (3)	6.0 (2)
C40	0.4304 (9)	0.0723 (6)	0.5745 (4)	4.3 (3)	F2	0.8449 (7)	0.0454 (4)	0.9757 (3)	8.2 (2)
C41	0.3884 (7)	0.0116 (5)	0.5872 (4)	2.9 (2)	F3	0.9495 (5)	0.0386 (4)	0.9282 (3)	6.8 (2)
C42	0.4058 (7)	−0.0126 (5)	0.6373 (4)	2.7 (2)	OW	0.7460 (4)	0.3160 (3)	0.7474 (2)	2.2 (1)

[a] Anisotropically refined atoms are given in the form of the isotropic equivalent displacement parameter defined as $(4/3)[a^2B(1,1) + b^2B(2,2) + c^2B(3,3) + ab(\cos\gamma)B(1,2) + ac(\cos\beta)B(1,3) + bc(\cos\alpha)B(2,3)]$.

Table II. Selected Bond Distances (Å), Bond Angles (deg), and Averages with Their Estimated Standard Deviations

Fe–N1	2.030 (5)	Fe–N23	2.011 (5)
Fe–N11	2.039 (5)	Fe–O1	2.188 (5)
Fe–N17	2.005 (5)	Fe–OW	2.133 (4)
N1–Fe–N11	88.9 (2)	N11–Fe–N23	179.3 (2)
N1–Fe–N17	178.3 (2)	N17–Fe–N23	89.8 (2)
N1–Fe–N23	90.9 (2)	O1–Fe–OW	175.5 (2)
N11–Fe–N17	90.3 (2)		
Porphyrin Mean Values[a]			
$N–C_\alpha$	1.383 (13)	$C_{phe}–N_{am}$	1.398 (13)
$C_\alpha–C_\beta$	1.427 (9)	$N_{am}–C_{am}$	1.370 (12)
$C_\beta–C_\beta$	1.354 (17)	$C_{am}–O$	1.223 (14)
$C_\alpha–C_m$	1.390 (16)	$C_{am}–C_{ter}$	1.515 (26)
$C_m–C_{phe}$	1.506 (12)	$C_{ter}–C_{ter}$	1.550 (50)
$N–C_\alpha–C_\beta$	109 (1)	$C_\alpha–C_m–C_\alpha$	124 (1)
$C_\alpha–C_\beta–C_\beta$	107 (1)	$C_\alpha–C_m–C_{phe}$	117 (2)
$N–C_\alpha–C_m$	125.9 (9)		
Triflate Mean Values			
S–O	1.450 (11)	S–CT	1.797 (8)
CT–F	1.317 (16)		

[a] C_α, C_β, C_m, C_{phe}, N_{am}, C_{am}, and C_{ter} stand for the α, β, methine, phenyl, amido, and *tert*-butyl carbons or nitrogens, respectively.

of minor disorder of this group. This *tert*-butyl group is also that which has the poorest contacts with the triflate anion. The bond lengths in the $CF_3SO_3^-$ ion are comparable to those observed previously,[22] S–O1 = 1.450 (5), S–O2 = 1.439 (6), S–O3 = 1.462 (6), S–CT = 1.797 (8), and C-F = 1.317 (8) Å.

Mixed-Spin Model

In this section, we first compile the effects of the quantum-mechanical mixture, due to spin–orbit coupling, between the $S = {}^5/_2$ and $S = {}^3/_2$ spin states in ferric iron porphyrins[23] on effective g values,[24] zero-field splittings,[23,24] effective magnetic momenta,[24] and hyperfine fields,[25] as monitored by EPR, magnetic susceptibility, and Mössbauer studies. Second, we discuss the applicability of the usual spin ($S = {}^5/_2$) Hamiltonian analysis of Mössbauer spectra in spin-mixed iron(III) complexes.

In a moderate crystal field of quasi-cubic symmetry with weak axial component in z direction, the energetically lowest electronic configurations of iron(III) follow from the 3d orbital occupations $(xy)^1\,(xz)^1\,(yz)^1\,(3z^2 - r^2)^1\,(x^2 - y^2)^1$ and $(xy)^2\,(xz)^1\,(yz)^1\,(3z^2 - r^2)^1$ and are denoted by $^6A_1$ and $^4A_2$ in C_{4v} symmetry.[23] The corresponding substates of the two spin multiplets with equal magnetic quantum numbers $m = \pm{}^1/_2$ and $m = \pm{}^3/_2$ interact via

(22) Prins, R.; Birker, P. J. W. L.; Haasnoot, J. G.; Verschoor, G. C.; Reedijk, J. *Inorg. Chem.* **1985**, *24*, 4128.
(23) Griffith, J. S. *The Theory of Transition Metal Ions*; Cambridge University Press: Cambridge, England, 1961.
(24) Maltempo, M. M.; Moss, T. H. *Q. Rev. Biophys.* **1976**, *9*, 181.
(25) Maltempo, M. M.; Moss, T. H.; Spartalian, K. *J. Chem. Phys.* **1980**, *73*, 2100.

spin–orbit coupling, $\lambda\sum\vec{s}_k\cdot\vec{l}_k$, with $\vec{s}_k$ and $\vec{l}_k$ being the one-electron spin- and orbital-momentum operators, and the summation over the 3d electrons. The interaction yields mixed-spin electronic eigenstates

$$|-,\pm m\rangle = a_m|^6A_1,\pm m\rangle + b_m|^4A_2,\pm m\rangle \quad (1a)$$

in the lower multiplet and

$$|+,\pm m\rangle = -b_m|^6A_1,\pm m\rangle + a_m|^4A_2,\pm m\rangle \quad (1b)$$

in the excited multiplet. The $|^6A_1,\pm{}^5/_2\rangle$ state remains of pure spin $S = {}^5/_2$. For a negative electrostatic term-energy splitting, $\Delta = E(^6A_1) - E(^4A_2) < 0$, the dominant spin in the low-energy state (eq 1a) is $S = {}^5/_2$ ($a_m^2 > {}^1/_2$), and accordingly, for positive Δ, $S = {}^3/_2$. The coefficients a_m and b_m can be calculated, for each value of m, by solving a 2×2 secular problem of the combined electrostatic and spin–orbit interaction. The diagonal elements of the Hamilton matrices are the electrostatic term energies of the $^6A_1$ and $^4A_2$ configurations; the off-diagonal elements are $c_m = -\lambda\sqrt{({}^6/_5)}$, $-\lambda\sqrt{({}^4/_5)}$, and 0 for $m = {}^1/_2$, ${}^3/_2$, and ${}^5/_2$, respectively.[23] The relative energies of the Kramers doublets are given by

$$E_m^{(0)\pm} = (\Delta \pm \sqrt{(\Delta^2 + 4c_m^2)})/2 \quad (2)$$

with the plus and minus sign referring to the excited (eq 1b) and low-energy (eq 1a) states, respectively. For large term splittings, $|\Delta| \gg \lambda$, the doublet energies of the lowest Kramers doublets are, in good approximation, described by the zero-field operator DS_z^2, with $D = |\lambda^2/5\Delta|$. The zero-field splitting D is, in the model, necessarily positive, and the ratio of the energy spacings, $E_{5/2}^{(0)-} - E_{3/2}^{(0)-}$ and $E_{3/2}^{(0)-} - E_{1/2}^{(0)-}$, between the three lowest doublets of dominant ground-state spin $S = {}^5/_2$ ($\Delta < 0$), is 2. Small term splittings, $|\Delta| \sim \lambda$, give rise to large zero-field splittings and to ratios of the energy spacings larger than 2. In the 10-state model for spin mixture discussed here, the rhombicity parameter E is zero.

A direct measure of the spin mixture in the ground-doublet states (eq 1a) is the effective g factor[24] $g_{1/2\perp}{}^- = 6a_{1/2}{}^2 + 4b_{1/2}{}^2$. The corresponding effective g factor of the excited state (eq 1b), $g_{1/2\perp}{}^+$, is obtained by interchanging $a_{1/2}$ and $b_{1/2}$ in the expression for $g_{1/2\perp}{}^-$. Substitution of the expressions of a_m and b_m in terms of Δ/λ yields for the effective g factors in the two $m = \pm{}^1/_2$ doublets the expression

$$g_{1/2\perp}{}^\gamma = 5 \pm 1/\sqrt{[1 + 24(\lambda/\Delta)^2/5]} \quad (3)$$

The plus and minus sign at the right-hand side of eq 3 refer to the Kramers doublet, γ, with the major $S = {}^5/_2$ and $S = {}^3/_2$ spin component, respectively.

The temperature dependence of the effective magnetic moment is in the temperature range $kT \gg \mu_B B$, B being the applied magnetic field, in good approximation given by the expression of Van Vleck[26]

$$\mu_{\text{eff}\alpha}{}^2 = \frac{3\sum[(E_{m\alpha}^{(1)\gamma})^2 - 2kTE_{m\alpha}^{(2)\gamma}]\exp(-E_m^{(0)\gamma}/kT)}{\sum\exp(-E_m^{(0)\gamma}/kT)} \quad (4)$$

The summations are over γ and m, with the index γ labeling the ground ($\gamma = -$) and excited ($\gamma = +$) states given in the expressions (1a) and (1b), respectively. The coefficients $E_{m\alpha}^{(i)\gamma}$ are the expansion coefficients of the energies of the Kramers doublet $|\gamma,m\rangle$ in powers of B_α ($\alpha = \perp$ or $\parallel$, i.e. perpendicular or parallel to the axial direction):

$$E_{m\alpha}{}^\gamma = E_m^{(0)\gamma} + B_\alpha E_{m\alpha}^{(1)\gamma} + B_\alpha{}^2 E_{m\alpha}^{(2)\gamma} \quad (5)$$

$E_m^{(0)\gamma}$ is the energy of the Kramers doublet, $|\gamma,m\rangle$, in absence of an applied field, $E_{m\alpha}^{(1)\gamma} = mg_{m\alpha}{}^\gamma\mu_B$ and $E_{m\parallel}^{(2)\gamma} = 0$. In our analysis, $E_{m\perp}^{(2)\gamma}$ was calculated by treating the Zeeman interaction of the perpendicular field component, $B_\perp$, between the Kramers doublets in second-order perturbation theory. Such a perturbative treatment is allowed, since $\mu_B B \ll D$ in the spin-mixed systems considered here. In our application of eq 4, $g_{1/2\perp}{}^\gamma$ is given by eq 3, $g_{3/2\perp}{}^\gamma = g_{5/2\perp}{}^\gamma = 0$, and $g_{m\parallel}{}^\gamma = 2$ for all values of m. In powder samples, μ_{eff} is obtained from the orientational average[24] $\mu_{\text{eff}}{}^2 = (\mu_{\text{eff}\parallel}{}^2 + 2\mu_{\text{eff}\perp}{}^2)/3$. In the range $kT \gg \mu_B B$, the result of Van Vleck's procedure (eq 4) for the evaluation of μ_{eff} is in close agreement with that obtained from the direct calculation of μ_{eff} in terms of temperature-averaged spin-expectation values or of field derivatives of the electron-state energies.[26]

In the evaluation of the Mössbauer spectra, the Hamiltonian, including the electrostatic term splitting, spin–orbit coupling term, and Zeeman interaction, is diagonalized within the 10-dimensional spin space spanned by the multiplets of spin $S = {}^5/_2$ and $S = {}^3/_2$. Subsequently, the magnetic hyperfine field at the iron nucleus in each of the electronic eigenstates, $\langle\gamma,m|\vec{B}_{\text{hf}}|\gamma,m\rangle$, was calculated by using[27]

$$\vec{B}_{\text{hf}} = \vec{B}_{\text{dip}} + \vec{B}_{\text{cont}} \quad (6a)$$

where

$$\vec{B}_{\text{dip}} = B_0{}^d\sum_k[3(\vec{r}_k\cdot\vec{s}_k)\vec{r}_k - \vec{s}_k] \quad (6b)$$

and

$$\vec{B}_{\text{cont}} = B_0{}^c\sum_k\vec{s}_k \quad (6c)$$

are, respectively, the dipolar and Fermi contact contributions to the internal field. The orbital contribution to the magnetic hyperfine field remains zero under spin mixture. The summations in eqs 6b and 6c are over the 3d electrons; $\vec{r}_k$ is a normalized electron-position vector. The coefficient $B_0{}^d$ can be expressed as $-2\mu_B\langle r^{-3}\rangle_{3d}$. From $\langle r^{-3}\rangle_{3d} \approx 4.6a_0{}^{-3}$, $B_0{}^d$ is found to be of the order -60 T.[27] The coefficient $B_0{}^c$ is conventionally written[27] as $-\kappa B_0{}^d$, with κ a dimensionless constant of about 0.35 in iron porphyrins. Within the 10-dimensional spin space considered, $\vec{B}_{\text{hf}}$ can be expressed as[25]

$$\vec{B}_{\text{hf}} = B_0{}^c\vec{S} + B_0{}^dP(-{}^4/_{21}S_x, -{}^4/_{21}S_\gamma, +{}^8/_{21}S_z)^TP \quad (7)$$

where P is the projection operator on the subspace of $S = {}^3/_2$ spin states. The Fermi contact term acts on both the $S = {}^5/_2$ and $S = {}^3/_2$ components of the wave functions, whereas the dipolar contributions only arise from the $S = {}^3/_2$ components. As a consequence of the opposite signs of $B_0{}^c$ (positive) and $B_0{}^d$ (negative), the dipolar contribution enhances the contact field in the x and y directions but weakens the field in the z direction.

The Mössbauer spectra were calculated, either in slow or in fast relaxation, by using a nuclear Hamiltonian containing, next to the electric quadrupole and nuclear Zeeman terms,[28] the magnetic hyperfine-coupling term $-g_N\mu_N\vec{B}_{\text{hf}}\vec{I}$, with g_N, μ_N, and $\vec{I}$ being the nuclear g factor, magneton, and angular momentum, respectively.

In the analysis of the Mössbauer spectra recorded at low temperatures ($kT \ll D$), one can also adopt the usual spin Hamiltonian ($S = {}^5/_2$)

$$H_e = D[S_z^2 - S(S+1)/3 + E(S_x^2 - S_y^2)/D] + \mu_B\vec{B}\cdot g'\cdot\vec{S} \quad (8)$$

instead of applying the 10-state model. The effects of the spin mixture are then lumped into the zero-field splitting D and the g' factors by taking $D = (E_{3/2}{}^{(0)-} - E_{1/2}{}^{(0)-})/2$, $g_\perp{}' = g_{1/2\perp}{}^-/3$, and $g_\parallel{}' = 2$.

At higher temperatures ($kT > D$), the zero-field operator has, in case of strong spin $S = {}^3/_2$ admixture, to be extended by a quartic term $D'S_z^4$. Moreover, the A tensor should then be made dependent on the Kramers doublet. By identifying the hyperfine term $-g_N\mu_N\langle\gamma,\pm m|\vec{B}_{\text{hf}}|\gamma,\pm m\rangle\cdot\vec{I}$ with the expression $g_N\mu_N\langle S = {}^5/_2,\pm m|S|S = {}^5/_2,\pm m\rangle\cdot\mathbf{A}_m{}^\gamma\cdot\vec{I}$, we can deduce a set of Kramers-

(26) van Vleck, J. H. *Theory of Electric and Magnetic Susceptibilities*; Oxford University Press: London, 1932.

(27) Abragam, A.; Bleaney, B. *Electron Paramagnetic Resonance of Transition Ions*; Dover Publications Inc.: New York, 1986.

(28) Gütlich, P.; Link, R.; Trautwein, A. X. *Mössbauer Spectroscopy and Transition Metal Chemistry*; Springer-Verlag: Berlin, 1978.

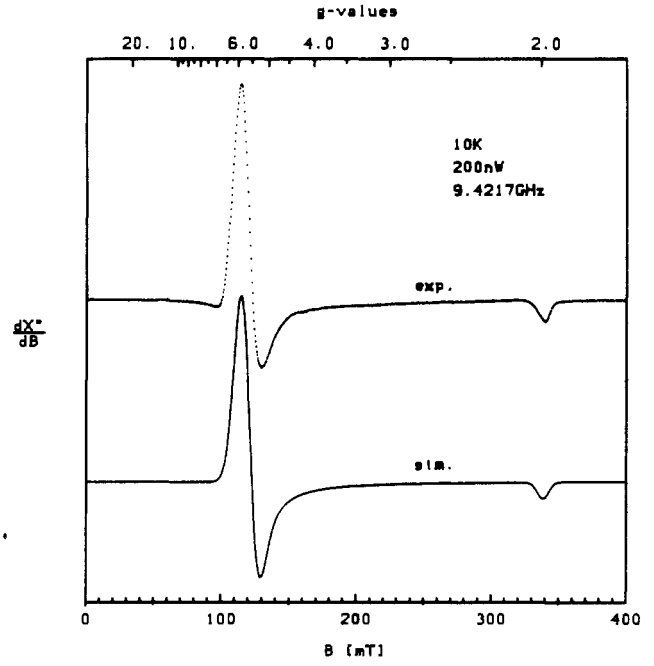

Figure 3. Experimental and simulated EPR spectrum of a polycrystalline sample of compound **1**. The simulation is based on a simple $S' = {}^1/_2$ formalism. The used effective g values are 5.7, 5.7, and 2.0. The line width was taken anisotropic 7.5, 7.5, and 5 mT, corresponding to the given g values.

doublet-dependent effective $\mathbf{A}_{m\alpha}{}^{\gamma}$ tensors. For the ground doublet we find, dropping the index γ

$$A_{1/2\perp} = -B_0{}^{c}\left(2 + a_{1/2}{}^{2}\right)/3 + 8B_0{}^{d}\left(1 - a_{1/2}{}^{2}\right)/63$$

$$A_{1/2\parallel} = -B_0{}^{c} - 8B_0{}^{d}\left(1 - a_{1/2}{}^{2}\right)/21 \qquad (9)$$

The coefficient $a_{1/2}{}^2$ can be directly expressed in terms of effective g values by $a_{1/2}{}^2 = (g_{1/2\perp}{}^{-} - 4)/2$. For large values of the zero-field splitting, $D \gg \mu_B B$, the spin expectation values calculated in the lowest $m = \pm{}^1/_2$ doublet are, for the major part of the crystal directions relative to the applied field, mainly oriented along the xy plane, whereas in the $m = \pm{}^3/_2$ and $m = \pm{}^5/_2$ doublets, the orientations are mainly along the z axis. The Mössbauer spectra are thus rather insensitive to the values of $A_{1/2\parallel}$, $A_{3/2\perp}$, and $A_{5/2\perp}$. The expression for $A_{3/2\parallel}$ follows from that of $A_{1/2\parallel}$ given in eq 9 by substituting $a_{3/2}$ for $a_{1/2}$. $A_{5/2\parallel}$ is equal to $B_0{}^{c}$, since the $m = \pm{}^5/_2$ doublet is of pure $S = {}^5/_2$ spin. The value of $A_{3/2\parallel}$ lies between the values for $A_{1/2\parallel}$ and $A_{5/2\parallel}$, because the degree of spin $S = {}^3/_2$ admixture in the Kramers doublet $m = \pm{}^3/_2$ lies between those in the $m = \pm{}^1/_2$ and $m = \pm{}^5/_2$ doublets. In the derivation of the expressions (9), it is assumed that the parameter $B_0{}^{c}$ is independent of the electronic terms $^6A_1$ and $^4A_2$. Differences in the delocalization properties of the orbitals occupied in these terms may, however, lead to different values for this parameter.

In practice, the fast relaxation, which occurs at temperatures where the excited levels are occupied, makes the simulated Mössbauer spectra rather insensitive to the refinements in the usual spin Hamiltonian analysis discussed above.

The effects of the quantum-mechanical spin mixture on the electronic structure parameters in ferric iron porphyrins, as discussed in terms of the 10-state model, can be summarized as follows: (a) The zero-field splitting D is positive, and the rhombicity parameter is zero. (b) The effective $g_\perp$ factor lies between 6 and 4. (c) The effective magnetic moment ranges correspondingly between 5.9 and 3.9 μ_B. (d) The A tensor is Kramers-doublet dependent, and anisotropic with $|A_{1/2\perp}| > |A_{1/2\parallel}|$.

Magnetic and Electronic Properties of 1

In this section we attempt to attain a consistent interpretation of the EPR, magnetic susceptibility, and Mössbauer data of compound **1**, in the framework of the mixed-spin model, discussed in the previous section, by using one common set of parameters.

Figure 3 depicts an X-band EPR spectrum, recorded on a polycrystalline sample of compound **1**, and a simulation, based on a computational routine for effective spin $S' = {}^1/_2$. The effective g values for this simulation are 5.7, 5.7, and 2.0, with anisotropic line widths 7.5, 7.5, and 5 mT, respectively. The small deviations between the simulation and the experiment, as well as the large, anisotropic line width, are attributed to spin–spin interaction in the densely packed crystal structure. The temperature dependence of the spectrum indicates that the signals originate from the lowest Kramers doublet. A comparison of the effective g values with the values 6, 6, and 2 of a pure $|S = {}^5/_2, m = \pm{}^1/_2\rangle$ Kramers doublet reveals a spin-mixed ground state with prevailing high-spin character. Substituting the value 5.7 for $g_{1/2\perp}{}^{-}$ in eq 3 yields the ratio $\Delta/\lambda = -2.15$.

The EPR spectra could also be simulated by adopting slightly reduced line widths together with rhombic splittings $\Delta g_\perp = g_x - g_y \leq 0.5$, in the $g_\perp$ resonances. From the first-order perturbation expression $\Delta g_\perp = 48E/D$, we find an upper limit for the rhombicity parameter $E/D \leq 0.01$, in accordance with the value $E/D = 0$, deduced from the 10-state model for spin mixture. A more accurate determination of E/D is not possible by means of the spectroscopies discussed here, because the Mössbauer spectra are even less sensitive to this parameter.

The magnetic susceptibility of compound **1** was recorded in the temperature range 2–300 K. The temperature dependence of the orientationally averaged effective momenta, calculated with the use of eq 4, was least-squares fitted to the data for μ_{eff} obtained from the cgs expression

$$\mu_{eff} = \sqrt{[8.0(\mathrm{MW}(\chi_{mass}) - \chi_{dia})T]} \qquad (10)$$

where χ_{mass} is the experimental mass susceptibility at temperature T, MW the molecular weight, and χ_{dia} the molar diamagnetic susceptibility of the compound. Since eq 4 is only valid for $kT \gg \mu_B B$, the fit was carried out in the range 10–300 K. Taking λ, Δ, and χ_{dia} as fit parameters and the molecular weight MW as deduced from the X-ray structure, the optimized values are found to be 227 cm^{-1}, −457 cm^{-1}, and -1807×10^{-6} cm^3/mol, respectively. The spin–orbit coupling parameter λ is strongly reduced compared with the free ion value,[27] $\lambda \sim 400$ cm^{-1}, indicating a considerable perturbation of the 3d orbitals of the iron ion. The resulting ratio $\Delta/\lambda = -2.01$ is close to the EPR value and yields for $g_{1/2\perp}{}^{-}$, by using eq 3, the value 5.68. Conversely, the value of $\mu_{eff}(300\ \mathrm{K}) = 5.66\ \mu_B$ evaluated for the EPR value $\Delta/\lambda = -2.15$ is only about 0.02 μ_B larger than the value of μ_{eff} calculated for $\Delta/\lambda = -2.01$. At higher temperatures ($\gtrsim$100 K), the spin-only value of μ_{eff} is determined by Δ/λ and runs from 3.9 μ_B ($S = {}^3/_2$) to 5.9 μ_B ($S = {}^5/_2$) by changing Δ/λ from minus to plus infinity. Subsequently, at temperatures $kT \gtrsim |\Delta|$, the thermal occupation of the upper Kramers doublets of the 10-state model leads to changes in μ_{eff}; however, in compound **1**, this effect is small in the temperature range considered.

The small difference between the values for Δ/λ inferred from g factors and magnetic momenta may originate from a vertical shift of the μ_{eff} vs T curve, caused by an inaccuracy in the molecular weight (see eq 10). In order to estimate the change in the molecular weight, relative to its X-ray structure value 1232.2, needed to explain the discrepancy between the two Δ/λ values, a least-squares fit of the μ_{eff} vs T curve was performed with MW, Δ, and χ_{dia} as fit parameters, while the ratio Δ/λ was kept fixed to the EPR value −2.15. The optimized values (see Table III) MW = 1249, $\Delta = -491$ cm^{-1}, $\lambda = 229$ cm^{-1}, and $\chi_{dia} = -1717 \times 10^{-6}$ cm^3/mol, are in close agreement with the values obtained in the former fit and imply a variation in the molar mass of 1.5% only. The experimental and theoretical temperature dependences of μ_{eff}, calculated with the latter parameter set, are given in Figure 4 and are found to be in excellent agreement. We note that slight variations in the high-temperature values of μ_{eff} may also originate from texture effects in the susceptibility measurements.

Substitution of the optimized values for Δ and λ, given in Table III, into eq 2 results in energy gaps $E_{5/2}{}^{(0)-} - E_{3/2}{}^{(0)-}$ and $E_{3/2}{}^{(0)-}$

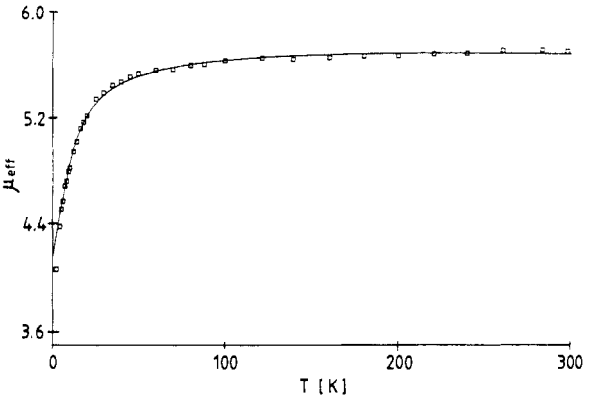

Figure 4. Temperature dependence of the effective magnetic moment, in units μ_B, of compound **1** in the range 2–300 K. The squares represent μ_{eff} as obtained, with eq 10, from the experimental mass susceptibilities by using the molar weight MW = 1249 Da and the diamagnetic susceptibility $\chi_{dia} = -1717 \times 10^{-6}$ cm^3/mol. The solid curve is the theoretical fit with expression 4, using the values of the parameters Δ and λ given in Table III.

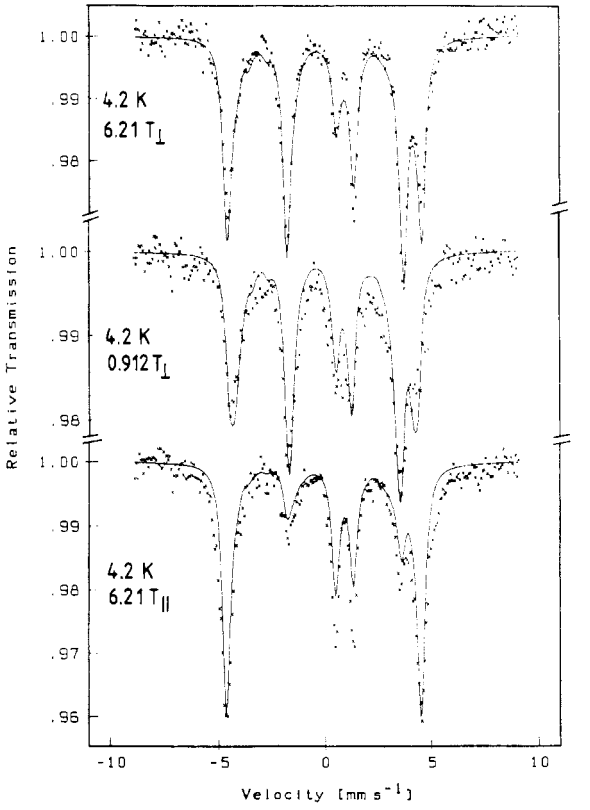

Figure 5. Mössbauer spectra of compound **1** recorded at 4.2 K in applied fields of (a) 6.21 T and (b) 0.912 T both perpendicular to the γ-beam and (c) 6.21 T parallel to the γ-beam. The solid lines represent the simulations, in the slow-relaxation mode, with the mixed-spin model, using the parameters given in Table III.

$-E_{1/2}^{(0)-}$ of 74 and 31 cm^{-1}, respectively. The ratio of the energy gaps is 2.37, so that the usual zero-field operator DS_z^2 is not strictly valid anymore.

The zero-field splitting, which is roughly proportional to λ^2/Δ, is a measure for the slope of the μ_{eff} vs T curve at lower temperatures. At temperatures $kT \leq \mu_B B$, the effective magnetic moment approaches zero, whereas μ_{eff}, as presented in eq 4, takes the spurious nonzero value $\sqrt{[(g_{1/2\parallel}^-)^2 + 2(g_{1/2\perp}^-)^2]/2}$, which is equal to 4.15 in Figure 4. The discrepancy is owing to the violation of the condition $kT \gg \mu_B B$ used in deriving eq 4.

Mössbauer spectra of compound **1** were recorded in powder samples at temperatures of 4.2–250 K in applied fields of 0–6.21 T, oriented parallel or perpendicular to the γ-beam.

Table III. Mixed-Spin Model Parameters and Corresponding Spin ($S = {}^5/_2$) Hamiltonian Parameters of Compound **1**

	Electronic Parameters		
Δ	−491 cm^{-1}	E/D	0
λ	229 cm^{-1}	$g_\perp$	5.7[b]
D	15.6 cm^{-1}[a]	$g_\parallel$	2.00[b]
	Hyperfine Parameters		
δ	0.43 mm s^{-1}[c,d]	B_0^c	17.7 to 16.8 T[g]
ΔE_Q	+2.2 mm s^{-1}[d]	B_0^d	−11.6 to −56.9 T[g]
η	0[e]	$A_{1/2\perp}$	−17.0 T
Γ	0.40 mm s^{-1}[f]	$A_{1/2\parallel}$	−17.0 to −13.5 T[g]

[a] Corresponds to half of the zero-field splitting between the lowest $m = \pm^1/_2$ and $\pm^3/_2$ Kramers doublets, as derived from the mixed-spin model. [b] Effective g factor, from EPR spectra recorded at 4.2 K. [c] Relative to α-Fe at room temperature. [d] Measured at room temperature. [e] Asymmetry parameter of the electric quadrupole interaction. [f] Line width used in Mössbauer analysis. [g] Range of possible $A_{1/2\parallel}$, and corresponding B_0^c and B_0^d values, according to the Mössbauer analysis. In the simulations given in Figures 5 and 6, B_0^c and B_0^d are taken as 16.8 and −56.9 T, respectively.

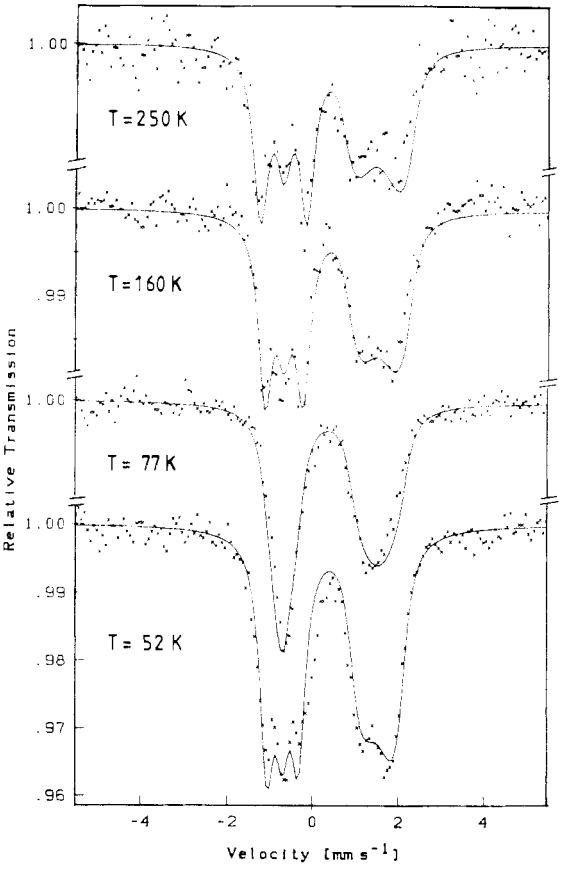

Figure 6. Mössbauer spectra of compound **1** recorded at temperatures ranging from 52 to 250 K in an applied field of 6.21 T perpendicular to the γ-radiation. The solid lines represent the simulations, in fast relaxation, with the mixed-spin model, using the parameters given in Table III.

The spectra without field exhibit, from 4.2 to 250 K, an almost temperature-independent quadrupole splitting $\Delta E_Q = 2.2$ mms^{-1} and isomer shift $\delta = 0.43$ mms^{-1}. The simulations of the spectra, given in Figures 5 and 6, were performed with the 10-state model for spin mixture by using the parameters Δ and λ given in Table III, which were obtained from the analysis of the EPR and the magnetic susceptibility data. The zero-field splittings are large compared to kT at 4.2 K and to $\mu_B B$ for all applied fields considered. The 4.2 K spectra (Figure 5) thus pertain to the lowest Kramers doublet $m = \pm^1/_2$. In such a system, the spin-expectation values, and the associated internal fields, reach their saturation value already for small fields ($B \sim 10$ mT). A further increase of the applied field from 0.912 to 6.20 T (Figure 5) leaves the internal field almost stationary, because the Zeeman interactions

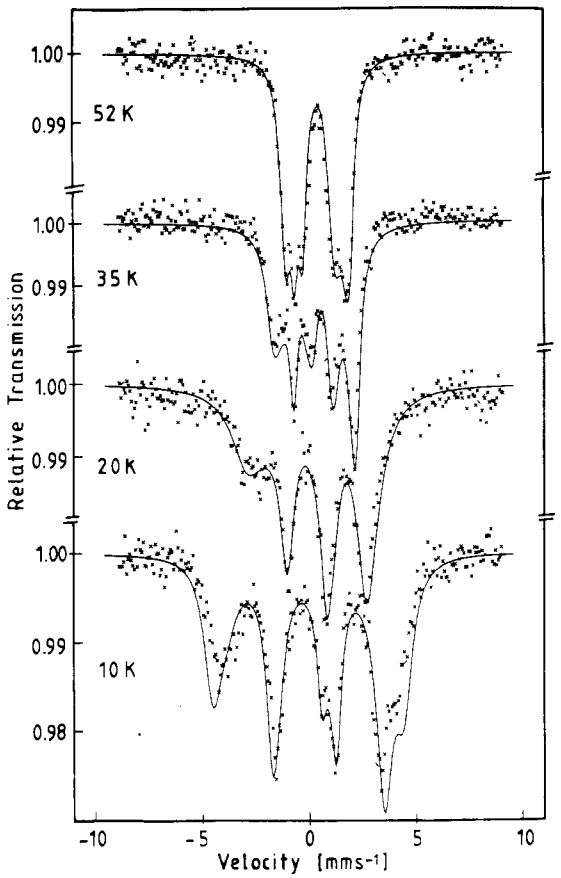

Figure 7. Mössbauer spectra of compound **1** recorded at temperatures ranging from 10 to 52 K in an applied field of 6.21 T perpendicular to the γ-radiation. The solid lines represent the simulations, taking into account spin–lattice relaxation with a relaxation constant $w_0^{SL} = 1.8 \times 10^4$ rad s^{-1} K^{-3}.

between the Kramers doublets are still small, compared with the zero-field splitting ($D \gg \mu_B B$). An accurate value of the zero-field splitting could not be determined from the 4.2 K Mössbauer spectra.

The magnetic hyperfine constants, B_0^c and B_0^d were determined from the hyperfine splittings in the 4.2 K spectra. First, the components of the A tensor were determined to be $A_{1/2\perp} = -17.0$ T and $A_{1/2\parallel} = -13.5$ up to -17.0 T by applying the usual spin ($S = {}^5/_2$) Hamiltonian analysis, with $D = 15.6$ cm^{-1} and $E/D = 0$. Substitution of the A-tensor components and of the value $a_{1/2} = 0.85$, deduced from $g_{1/2\perp}^- = 5.7$, into eq 9, and solving B_0^c and B_0^d, leads correspondingly to the values $B_0^c = 16.8$ up to 17.7 T and $B_0^d = -56.9$ up to -11.6 T (Table III). The values of the corresponding A-tensor components in the $m = \pm{}^3/_2$ and $\pm{}^5/_2$ doublets, $A_{3/2\parallel}$ and $A_{5/2\parallel}$, are -14.2 up to -17.1 and -16.8 up to -17.7 T, respectively. Since the lower bound for B_0^d (-56.9 T) accords with theoretical estimates for the quantity, this value was used in the simulations presented in Figures 5 and 6.

A deeper insight into the properties of the ground-state multiplet can be gained if effects of intermediate relaxation are allowed for in the analysis. The predominant mechanism is supposed to be spin–lattice relaxation. This is suggested by inspection of Figure 7, where, in an applied field of 6.21 T, a successive broadening of the lines in the 10 and 20 K spectra is observed relative to the corresponding spectrum in Figure 6 taken at 4.2 K. At $T = 35$ K the onsetting collapse of the hyperfine splitting is already visible, while the temperature $T = 52$ K, chosen for the registration of the fourth spectrum, is high enough to admit the interpretation of that spectrum by using the fast-relaxation approach.

The simulations entered as solid lines into Figure 7 are based on stochastic theory of line shape by Clauser and Blume.[29] The transition probabilities between any pair of electronic states $|i\rangle$ and $|j\rangle$ with energies $E_i < E_j$, which are induced by the absorption of a phonon, are taken to be given by[30]

$$w_{ij} = w_0^{SL} T_{ij}^3 / [\exp(T_{ij}/T) - 1]$$

with rate constant

$$w_0^{SL} = 3k^3 |V^{(1)}|^2 / (2\pi\hbar^4 v^5 \rho) \qquad (11)$$

and

$$T_{ij} = |E_i - E_j|/k$$

Here, the phonon distribution is described in the Debye approximation, ρ is the mass density, and v is an average speed of sound in the material. $|V^{(1)}|$ is the transition matrix element, which, because of the lack of any further information about its explicit form, is taken independent of the states involved. The rate of the reverse transition, which is accompanied by the emission of a phonon, is determined by the principle of detailed balance such that

$$w_{ji} = w_{ij} p_i / p_j$$

where

$$p_i = \exp(-E_i/kT) / \sum_k \exp(-E_k/kT)$$

is the Boltzmann population of the electronic state $|i\rangle$. The simulations in Figure 7 have been calculated as outlined in ref 31 with $w_0^{SL} = 1.8 \times 10^4$ rad s^{-1} K^{-3}. Also spectra that were taken in an applied magnetic field of 0.912 T (not shown here) could be simulated satisfactorily with the same rate constant.

Favorable conditions for the precise determination of the zero-field splitting are found at weak applied fields. These split the Kramers doublets only little without mixing them. Between the two substates of the $\pm{}^1/_2$ ground state as well as of the $\pm{}^3/_2$ excited-state doublet, rapid relaxation is to be expected. The resulting magnetic hyperfine field generated by the $\pm{}^1/_2$ doublet points, as stated earlier, perpendicular to the molecular z axis, while the $\pm{}^3/_2$ doublet gives rise to a component parallel to the z axis, which grows with rising temperature. The temperature-dependent Mössbauer spectra consist therefore of a quadrupole-split resonance with the one or the other of the two lines broadened by the magnetic hyperfine interaction. The temperature at which equal intensity of the two lines is observed depends sensitively on the energetic distance between the two Kramers doublets and thus on the zero-field splitting. In Figure 8, Mössbauer spectra taken at various temperatures in an applied field of 12 mT are displayed. The simulations have been performed with the spin ($S = {}^5/_2$) Hamiltonian parameters given in Table III. The overall agreement with the experimental spectra confirms the validity of these values, notably of the zero-field splitting. The resulting spin–lattice relaxation constant $w_0^{SL} = 9 \times 10^3$ rad s^{-1} K^{-3} has only half the value found for the high-field spectra. Obviously, the assumption that the transition matrix elements are completely independent of the states involved is too coarse. Furthermore, the relaxation behavior could not be explained solely by spin–lattice relaxation, but at temperatures below 30 K, where it would become slow, spin–spin relaxation processes, visible also in the EPR line widths, come into play.

The transition probabilities between pure Zeeman levels due to spin–spin relaxation are given by the expression[32]

$$w(M \rightarrow M \pm 1) = {}^1/_4 w_0^{ss} |\langle M \pm 1 | S_\pm | M \rangle|^4 \rho(M \pm 1)$$

where the spin–spin relaxation constant

$$w_0^{ss} = \frac{2\pi}{\hbar} \sum_j (B_j + J_j)^2 P(E)$$

(29) Clauser, M. J.; Blume, M. *Phys. Rev. B* **1971**, *3*, 583.

(30) Winkler, H.; Schulz, C.; Debrunner, P. G. *Phys. Lett.* **1979**, *69A*, 360.

(31) Winkler, H.; Bill, E.; Trautwein, A. X.; Kostikas, A.; Simopoulos, A.; Terzis, A. *J. Chem. Phys.* **1988**, *89*, 732.

(32) Blume, M. *Phys. Rev.* **1968**, *174*, 351.

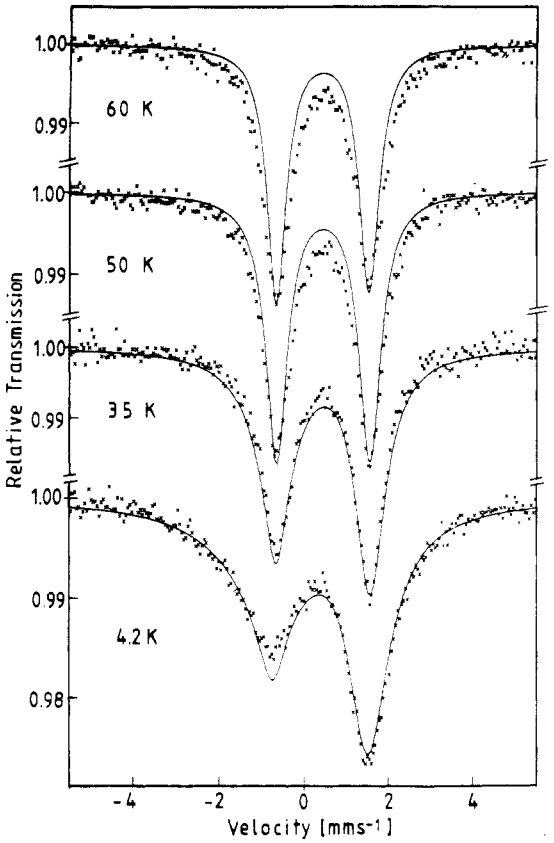

Figure 8. Mössbauer spectra of compound **1** recorded at temperatures ranging from 4.2 to 60 K in an applied field of 12 mT perpendicular to the γ-radiation. The solid lines represent the simulations, taking into account spin–spin relaxation with a relaxation constant $w_0^{ss} = 4.4 \times 10^7$ rad s^{-1} for the 4.2 K spectrum and spin–lattice relaxation with $w_0^{SL} = 9 \times 10^3$ rad s^{-1} K^{-3} for the other spectra.

contains the dipole–dipole and exchange-coupling constants B_j and J_j, respectively, of the Mössbauer ion with all its neighbors as well as its level density $P(E)$, while $\rho(M)$ are the Boltzmann populations of the magnetic substates of the neighbors.

In simulations w_0^{ss} is to be treated as an empirical parameter and expected to be independent of temperature and magnetic field. From the spectrum taken at 4.2 K the value of the spin–spin relaxation constant is determined as $w_0^{ss} = 4.4 \times 10^7$ rad s^{-1}. From this the coupling strength can be estimated if one makes a reasonable guess about $P(E)$, which is about the inverse of the electronic level width. Taking 1 cm^{-1} for the latter, one arrives at a value of 6×10^{-3} cm^{-1} for the spin–spin coupling, which corresponds to 2 μ_B at a distance of 4–5 Å.

Discussion

The systematic study of porphyrin derivatives, during the last two decades, has resulted in the discovery of a number of spin-state/stereochemical relationships.[33] An example is the relation between the Fe–N_p distance and the ground-state spin; viz., in high-spin ($S = {}^5/_2$) complexes the distance is systematically larger than in intermediate- ($S = {}^3/_2$) and low-spin ($S = {}^1/_2$) compounds. In five-coordinate high-spin complexes the increase in the Fe–N_p distance is associated with an out-of-plane displacement of the iron ion. The longer Fe–N_p separations (>2.040 Å),[33,34] occurring in six-coordinate high-spin complexes, arise from an expansion of the porphyrinato core. The mean Fe–N_p distance in six-coordinate low-spin compounds lies close to 1.990 Å. In systems with mixed-spin $S = {}^5/_2, {}^3/_2$ ground states, the average Fe–N_p distances are between 1.990 and 2.001 Å. These trends are

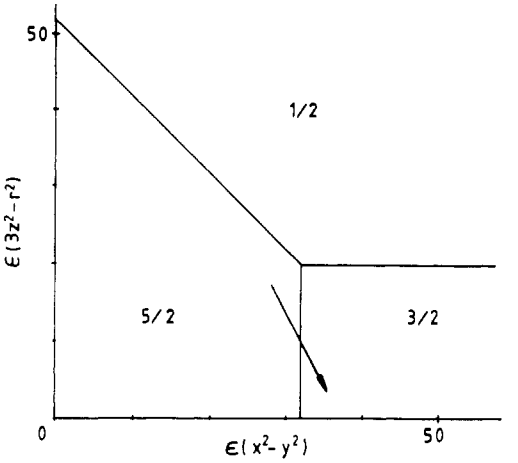

Figure 9. Schematic representation of the ground-state spin of tetragonally distorted ferric iron as a function of the electrostatic energies of the e_g orbital levels relative to the t_{2g} orbital levels. Splittings in the t_{2g} levels are neglected. The Racah parameters B and C are taken as 1100 and 3500 cm^{-1}, respectively. Energies are given in units of 10^3 cm^{-1}. The arrow indicates the proposed[7] behavior of ferric iron porphyrin complexes under weakening of the axial ligand field. Near the border line $S = {}^5/_2, {}^3/_2$, spin–orbit coupling leads to a strong spin mixture. Note that a decrease of $\epsilon(3z^2 - r^2)$ alone is not sufficient for a transfer from high to intermediate spin; a simultaneous change in the bonding between iron and the porphyrin ligand (increase of $\epsilon(x^2 - y^2)$) is required for a spin transition. Compound **1** is 491 cm^{-1} left from the vertical border line $S = {}^5/_2, {}^3/_2$.

attributed to the depopulation of the antibonding $3d_{x^2-y^2}$ orbital in states of lower spin.[33] Since these relationships have been proposed as a "final arbiter" of the spin state,[33] it is of interest to consider their prediction for the spin state in compound **1**. The average Fe–N_p distance 2.021 (16) Å found in **1** lies between the lower and upper bound of the Fe–N_p distance ranges in high-spin and intermediate-spin complexes, respectively, and implies a larger spin $S = {}^3/_2$ admixture than in high-spin compounds. Although this prediction is in accord with the effective g values and effective magnetic momenta observed in compound **1**, its nature is rather qualitative in view of the relatively large error margins in the X-ray data for the Fe–N_p distances. The axial coordination and the degree of the spin mixture deduced from the g values in compound **1** ($g_\perp = 5.7$) and the two structurally related complexes $[Fe(TPP)(H_2O)_2]^+$ ($g_\perp \approx 6$) and $[Fe(TPP)(OSO_2CF_3)]$ ($g_\perp \approx 5$) fit into the putative spin-state/stereochemical relationship visualized by Figure 9. The axial ligand field in **1** is weaker than that in the high-spin compound $[Fe(TPP)(H_2O)_2]^+$ because (i) the Fe–O(water) distance (2.133 (5) Å) in compound **1** is longer than that in $[Fe(TPP)(H_2O)_2]^+$ (2.095 Å)[20] and (ii) the triflate is considered to be a weaker field ligand than water.[7,19] Consequently, according to the relationship, the $S = {}^3/_2$ spin component in the ground state of compound **1** must be larger than that in $[Fe(TPP)(H_2O)_2]^+$, which is indeed in agreement with the spin mixture deduced from the g values 5.7 and ≈6, respectively, in the two complexes. On the other hand, the $S = {}^3/_2$ spin component in the ground state of compound **1** is smaller than that in the five-coordinate mixed-spin compound $[Fe(TPP)(OSO_2CF_3)]$ ($g_\perp \approx 5$),[7] as a consequence of the additional water ligand in **1**. The effective magnetic moment μ_{eff} at 300 K (5.66 μ_B) and the effective $g_\perp$ value (5.7) in compound **1** are larger than the values found in the quantum-mechanically mixed-spin systems $[Fe(TPP)(ClO_4)]$ (5.2 μ_B, 4.75),[7] $[Fe(OEP)(ClO_4)]$ (4.8 μ_B),[3] $[Fe(OEP)(C_2H_5OH)_2]^+$ (4.5 μ_B),[3] and $[Fe(TPP)(C(CN)_3)_2]$ (5.4 μ_B, 5.26)[4] and the monoclinic form of $[Fe(OEP)(3\text{-}Cl\text{-}py)_2]^+$ (4.5 μ_B, 4.9),[5] which indicates that the ground state in **1** has less $S = {}^3/_2$ character than in the five other complexes.

The quadrupole splitting in compound **1**, $\Delta E_Q \approx 2.2$ mm s^{-1}, lies between the values for this quantity observed in five-coordinate high-spin (0.5–0.8 mm s^{-1}) and five-coordinate mixed- or intermediate-spin (3.0–3.6 mm s^{-1})[20] heme derivatives and is larger than the values found in the six-coordinate ferric high-spin com-

(33) Scheidt, W. R.; Reed, C. A. *Chem. Rev.* **1981**, *81*, 543.
(34) Scheidt, W. R.; Gouterman, M. In *Iron Porphyrins*; Lever, A. B. P., Gray, H., Eds.; Addison-Wesley Publ. Co.: London, 1983; Part I.

pounds $[Fe(TPP)(TMSO_2)]^+$ (1.2 mm s^{-1})[35] and $[Fe(TPP)(H_2O)_2]^+$ (1.6 mm s^{-1})[20] and slightly smaller than that in the six-coordinate, spin-mixed, monoclinic form of $[Fe(OEP)(3\text{-}Cl\text{-}py)_2]^+$ (2.7 mm s^{-1}).[5] The contact-field parameter in compound **1**, B_0^c = 17 T, is about 1.5 T below the low-field side of the range of internal fields in high-spin heme derivatives[35] but is considerably larger than the value of 12 T deduced from low-temperature Mössbauer spectra in spin-mixed Chromatium ferricytochrome c′ (pH 7.8)[25] and in $[Fe(OEP)(3\text{-}Cl\text{-}py)]^+$ dimers.[36] The values of the g factors and zero-field-splitting and A-tensor components in compound **1** resemble those in the protein states I and II of *Rhodospirillum rubrum* ferricytochrome c′.[37] The quadrupole splitting in compound **1**, however, is significantly larger than the values ΔE_Q = 1.35 and 1.65 mm s^{-1} in the two protein states I and II, respectively.

Summing up the magnetic, electronic, and structural data, we conclude that the (triflato) aquoiron(III) "picket-fence" porphyrin compound **1** has a weakly spin-mixed ground state, with slightly more $S = {}^3/_2$ character than in high-spin ferric porphyrin derivatives.

Acknowledgment. R.W. is the recipient of an Alexander von Humboldt Award and thanks the Alexander von Humboldt Foundation for financial support. We thank Dr. Jacobi and Professor Gütlich from the Institut für Anorganische und Analytische Chemie, Johannes Gutenberg Universität, Mainz, FRG, for performing the magnetic susceptibility measurements.

Supplementary Material Available: Tables SI-SIV, listing thermal parameters for anisotropic atoms, hydrogen atom positions and thermal parameters, complete bond distances, and complete bond angles (11 pages); Table SV, listing observed and computed structure factor amplitudes (×10) for all observed reflections (19 pages). Ordering information is given on any current masthead page.

(35) Mashiko, T.; Kastner, M. E.; Spartalian, K.; Scheidt, W. R.; Reed, C. A. *J. Am. Chem. Soc.* **1978**, *100*, 6354.
(36) Gupta, G. P.; Lang, G.; Scheidt, W. R.; Geiger, D. K.; Reed, C. A. *J. Chem. Phys.* **1986**, *85*, 5212.
(37) Emptage, M. H.; Zimmermann, R.; Que, L.; Münck, E.; Hamilton, W. D.; Orme-Johnson, W. H. *Biochim. Biophys. Acta* **1977**, *495*, 12.

Contribution from the Department of Chemistry, University of Houston, Houston, Texas 77204-5641

Electrochemistry, Spectroscopy, and Reactivity of (*meso*-Tetrakis(1-methylpyridinium-4-yl)porphinato)cobalt(III,II,I) in Nonaqueous Media

C. Araullo-McAdams and K. M. Kadish*

Received January 23, 1989

The spectral and electrochemical properties of (*meso*-tetrakis(1-methylpyridinium-4-yl)porphinato)cobalt(II), $[(TMpyP)Co]^{4+}$, were investigated in dimethylformamide, dimethyl sulfoxide, and pyridine. A single one-electron oxidation of the complex involves a conversion of Co(II) to Co(III) and occurs in the range of +0.29 to −0.01 V vs SCE. Up to four electroreduction processes are also observed, and $[(TMpyP)Co]^{4+}$ can be reduced by a total of six electrons to generate $[(TMpyP)Co]^{2-}$ as a final product. The first reduction occurs between −0.49 and −0.61 V and leads to $[(TMpyP)Co^{I}]^{3+}$. The second reduction involves an addition of one electron to the porphyrin π-ring system and produces $[(TMpyP)Co^{I}]^{2+}$. However, electrochemical, spectroelectrochemical, and ESR monitoring of this reaction give data consistent with the occurrence of an intramolecular electron transfer involving electrogenerated $[(TMpyP)Co^{I}]^{2+}$ to form $[(TMpyP)Co^{II}]^{2+}$ in solution. Two additional reactions of $[(TMpyP)Co]^{2+}$ occur at $E_{1/2}$ values between −0.89 and −1.10 V, and these involve an overall four-electron reduction of the four *N*-methylpyridiniumyl substituents on TMpyP. The axial ligand binding reactions of pyridine with $[(TMpyP)Co]^{5+}$, $[(TMpyP)Co]^{4+}$, $[(TMpyP)Co]^{3+}$, and $[(TMpyP)Co]^{2+}$ were monitored by electrochemistry and ESR spectroscopy, and the ESR spectra of $[(TMpyP)Co(S)]^{4+}$, $[(TMpyP)Co(py)(S)]^{4+}$, $[(TMpyP)Co(py)_2]^{4+}$, $[(TMpyP)Co(py)]^{2+}$ and $[(TMpyP)Co(py)_2]^{2+}$ are presented where S = DMF or Me_2SO.

Introduction

The electroreduction of numerous cobalt porphyrins in nonaqueous media has been described in the literature.[1-12] The most prevalent reduction mechanism, which occurs in virtually all cases, involves a direct electron addition at the Co(II) center to form a Co(I) complex. A second electron is then added to the porphyrin π-ring system and leads to formation of a cobalt(I) porphyrin π anion radical.

The only cobalt(I) porphyrin dianion that has been characterized is $[((CN)_4TPP)Co]^{3-}$. This compound is electrogenerated from $((CN)_4TPP)Co$ and proceeds via an initial one-electron addition to the porphyrin π-ring system to form a cobalt(II) anion radical.[8] The potential for this reaction varies between −0.24 and −0.51 V depending upon solvent and is anodically shifted by as much as 1600 mV with respect to the first π-ring-centered reduction of (TPP)Co under the same solution conditions. The second reduction of $((CN)_4TPP)Co$ involves the Co(II) center and generates the cobalt(I) porphyrin π anion radical at $E_{1/2}$ values between −0.80 and −0.94 V. The third one-electron reduction occurs at −1.72 to −1.78 V and generates the Co(I) dianion. This reaction is very well-defined and has been characterized in a number of solvents.[8]

Several other easily reducible metalloporphyrins have been investigated in non-aqueous media. $[(TMpyP)M]^{4+}$ complexes, where TMpyP is *meso*-tetrakis(1-methylpyridinium-4-yl)porphyrin and M = Zn(II), Cu(II), or VO, are monomeric in DMF and can be reversibly reduced by a total of six electrons in three steps.[13] The first reduction involves a two-electron transfer at the porphyrin π-ring system and occurs at potentials that are positively shifted

(1) Kadish, K. M. *Prog. Inorg. Chem.* **1986**, *34*, 435-605.
(2) Guilard, R.; Kadish, K. M. *Chem. Rev.* **1988**, *88*, 1121-1146.
(3) Giraudeau, A.; Callot, H. J.; Jordan, J.; Ehzar, I.; Gross, M. *J. Am. Chem. Soc.* **1979**, *101*, 3857.
(4) Dolphin, D.; Halko, D. J.; Johnson, E. *Inorg. Chem.* **1981**, *20*, 2982.
(5) Wolberg, A.; Manassen, J. *J. Am. Chem. Soc.* **1970**, *92*, 2982.
(6) Walker, F. A.; Beroiz, D.; Kadish, K. M. *J. Am. Chem. Soc.* **1976**, *98*, 3484.
(7) Felton, R. H.; Linschitz, J. *J. Am. Chem. Soc.* **1966**, *88*, 1113.
(8) Lin, X. Q.; B.-Cocolios, B.; Kadish, K. M. *Inorg. Chem.* **1986**, *25*, 3242.
(9) Kadish, K. M.; Mu, X. H.; Lin, X. Q. *Inorg. Chem.* **1988**, *27*, 1489.
(10) Truxillo, L. A.; Davis, D. G. *Anal. Chem.* **1975**, *47*, 2260.
(11) Kadish, K. M.; Bottomley, L. A.; Beroiz, D. *Inorg. Chem.* **1978**, *17*, 1124.
(12) Kadish, K. M.; Bottomley, L. A.; Kelly, S.; Schaeper, D.; Shiue, L. R. *Bioelectrochem. Bioenerg.* **1981**, *8*, 213.
(13) Kadish, K. M.; Araullo, C.; Maiya, C. G.; Sazou, D.; Barbe, J.-M.; Guilard, R., *Inorg. Chem.* **1989**, *28*, 2528.

0020-1669/90/1329-2749$02.50/0